Check for updates

Geophysical Research Letters

RESEARCH LETTER
10.1029/2020GL092260

A Pronounced Spike in Ocean Productivity Triggered by the Chicxulub Impact

Julia Brugger[1,2,3], **Georg Feulner**[1], **Matthias Hofmann**[1], **and Stefan Petri**[1]

[1]Earth System Analysis, Potsdam Institute for Climate Impact Research, Member of the Leibniz Association, Potsdam, Germany, [2]Institute of Physics and Astronomy, University of Potsdam, Potsdam-Golm, Germany, [3]Senckenberg Biodiversity and Climate Research Centre (SBiK-F), Frankfurt, Germany

Key Points:

- We investigate the effects of sulfate aerosols, carbon dioxide and dust produced by the Chicxulub impact on climate and the marine biosphere
- Nutrients from the deep ocean and the projectile induce a short increase in marine primary productivity after the impact-induced darkness
- Simulated post-impact warming and carbon isotope changes indicate substantial emissions of carbon from the terrestrial biosphere

Supporting Information:

Supporting Information may be found in the online version of this article.

Correspondence to:

J. Brugger and G. Feulner,
brugger@pik-potsdam.de;
feulner@pik-potsdam.de

Citation:

Brugger, J., Feulner, G., Hofmann, M., & Petri, S. (2021). A pronounced spike in ocean productivity triggered by the Chicxulub impact. *Geophysical Research Letters*, *48*, e2020GL092260. https://doi.org/10.1029/2020GL092260

Received 23 DEC 2020
Accepted 24 MAY 2021

© 2021. The Authors.
This is an open access article under the terms of the Creative Commons Attribution License, which permits use, distribution and reproduction in any medium, provided the original work is properly cited.

Abstract There is increasing evidence linking the mass-extinction event at the Cretaceous-Paleogene boundary to an asteroid impact near Chicxulub, Mexico. Here we use model simulations to explore the combined effect of sulfate aerosols, carbon dioxide and dust from the impact on the oceans and the marine biosphere in the immediate aftermath of the impact. We find a strong temperature decrease, a brief algal bloom caused by nutrients from both the deep ocean and the projectile, and moderate surface ocean acidification. Comparing the modeled longer-term post-impact warming and changes in carbon isotopes with empirical evidence points to a substantial release of carbon from the terrestrial biosphere. Overall, our results shed light on the decades to centuries after the Chicxulub impact which are difficult to resolve with proxy data.

Plain Language Summary The sudden disappearance of the dinosaurs and many other species during the end-Cretaceous mass extinction 66 million years ago marks one of the most profound events in the history of life on Earth. The impact of a large asteroid near Chicxulub, Mexico, is increasingly recognized as the trigger of this extinction, causing global darkness and a pronounced cooling. However, the links between the impact and the changes in the biosphere are not fully understood. Here, we investigate how life in the ocean reacts to the perturbations in the decades and centuries after the impact. We find a short-lived algal bloom caused by the upwelling of nutrients from the deep ocean and nutrient input from the impactor.

1. Introduction

During its more than half a billion year long history, the evolution of animal and plant life on Earth was repeatedly disrupted by major mass-extinction events (Bambach, 2006). Among these biodiversity crises, the extinction at the Cretaceous-Paleogene (K-Pg) boundary (Renne et al., 2013) is unique: On the one hand, it is similar to many other mass-extinction events because of its association with continental flood basalt eruptions (Ernst & Youbi, 2017), in this case forming the Deccan Traps large igneous province in India (Schoene et al., 2019). On the other hand, it is the only extinction event which has been convincingly linked to an asteroid impact (Alvarez et al., 1980; Kring, 2007; Schulte et al., 2010), despite the fact that such large impacts with potentially global effects are statistically expected to occur once every 100–150 million years (Schmieder & Kring, 2020).

Initially put forward four decades ago (Alvarez et al., 1980), the hypothesis that the impact of a ~10 km asteroid was the main cause of the end-Cretaceous mass extinction event is now supported by multiple lines of evidence (Schulte et al., 2010). Particularly over the last few years, a number of studies on the events around the Cretaceous-Paleogene boundary have shed light on several important aspects. High-precision dating of zircons established the timing of the Deccan Trap eruptions (Schoene et al., 2019), indicating major pulses of volcanic activity ~50 kyr before and ~150 kyr after the impact, limiting their contribution to the extinction event which coincides with the impact. Data from the recent crater drilling project illuminate the immediate aftermath of the impact (Gulick et al., 2019) and, combined with improved geodynamic models, suggest a steeply inclined impact releasing significant amounts of carbon and sulfur from sedimentary rocks (Artemieva et al., 2017; Collins et al., 2020). Climate model simulations show that the formation of stratospheric sulfate aerosols leads to a colder and longer impact winter (Brugger et al., 2017) compared to the effects of impact dust alone. High-resolution proxy data confirm a pronounced short-term

surface ocean cooling in the months to decades after the impact (Vellekoop et al., 2014, 2016), followed by longer-term warming (Vellekoop et al., 2014, 2018). Furthermore, proxy studies report rapid ocean acidification which likely started in the century after the impact and lasted for several thousand years (Henehan et al., 2019). The breakdown of the $\delta^{13}C$ gradient from the surface to the deep ocean (Henehan et al., 2019; Sepúlveda et al., 2019; Zachos et al., 1989) probably indicates severe changes in the ocean's biological pump, but the detailed processes are still poorly understood. In particular, the immediate consequences of the impact on marine productivity during the first years to centuries after the impact cannot be reconstructed by proxy data due to a lack in temporal resolution.

Model experiments simulating the effects of sulfate aerosols from the impact on the climate indicate severe cooling resulting in strong ocean convection (Brugger et al., 2017). The resulting upwelling of nutrients from the deep ocean could increase marine primary productivity following the period of post-impact darkness, but it is unclear whether productivity remains limited by other critical nutrients (in particular iron) and how the marine biosphere is affected by the combined changes in light, temperature, ocean circulation, and nutrient distribution. Here, we address this question by modeling immediate impact-induced changes in climate and nutrient supply and their repercussions for the marine biosphere.

2. Materials and Methods

2.1. Model

We use the Earth-system model of intermediate complexity CLIMBER-3α+C (Hofmann et al., 2019; Montoya et al., 2005). The ocean model is a modified version of MOM3 (Hofmann & Morales Maqueda, 2006; Pacanowski & Griffies, 1999), run at a horizontal resolution of 3.75° x 3.75° with 24 vertical levels of variable thickness. Additionally, CLIMBER-3α+C includes a sub-model (Hofmann et al., 2019) which is similar to HAMOCC3.1 (Six & Maier-Reimer, 1996) and accounts for the dynamics of marine biogeochemistry and the carbon cycle. The stable carbon isotope fractionation of phytoplankton is parameterized as a function depending on the concentration of aquatic carbon dioxide (Hofmann et al., 1999), while for the inorganic carbonate system and the air-sea gas exchange the approach by Maier-Reimer (Maier-Reimer, 1993) is used. The sea-ice model (Fichefet & Maqueda, 1997) is a dynamic/thermodynamic model in two dimensions with the same horizontal resolution as the ocean model. The statistical-dynamical atmosphere model (Petoukhov et al., 2000) has a coarse resolution of 22.5° in longitude and 7.5° in latitude; it contains a module to simulate terrestrial sources, atmospheric transport and deposition of dust (Bauer & Ganopolski, 2010; Hofmann et al., 2019). The model version used for this study includes an improved lapse rate parametrization and more realistic ice and snow albedo values (Feulner & Kienert, 2014).

2.2. Boundary Conditions and Pre-Impact Climate State

An equilibrium simulation of the end-Cretaceous climate is the basis of all impact simulations. This equilibrium state is modeled using a Maastrichtian (70 Ma) continental configuration and vegetation distribution (Sewall et al., 2007), a solar constant of 1354 W/m^2, based on the present-day solar constant of 1361 W/m^2 (Kopp & Lean, 2011) and a standard solar model (Bahcall et al., 2001), and idealized orbital parameters (circular orbit, obliquity 23.5°). Proxy data for the Late Cretaceous give a wide range of CO_2 concentrations ranging from 240 ppm (Foster et al., 2017; Nordt et al., 2003) to 1,500 ppm (Royer, 2006). For the time just before the impact, there is evidence that atmospheric CO_2 concentrations were below 800 ppm (Foster et al., 2017; Hong & Lee, 2012; Nordt et al., 2002, 2003; Royer et al., 2012). We have adjusted the carbonate chemistry in the ocean to yield atmospheric CO_2 levels close to 500 ppm, a medium value within the range of proxy estimates: Starting from close to pre-industrial conditions (≈280 ppm), we have modified the ocean's alkalinity until the model approaches equilibrium at a value of 502 ppm after 11,400 model years. The equilibrium pre-impact state has a total alkalinity of 2,348 μeq L^{-1} and global annual mean amounts of dissolved inorganic carbon (DIC) of 2,328 μmol L^{-1}, of inorganic phosphate of 2.28 μ mol L^{-1} and silicate of 81.4 μ mol L^{-1}. For comparison, the measured present-day values are 2,353 μeq L^{-1} for the total alkalinity, 2,241 μ mol L^{-1} for DIC (Key et al., 2004), 2.1 μ mol L^{-1} for phosphate and 88.2 μ mol L^{-1} for silicate (objectively analyzed climatologies, Garcia et al., 2018). In addition to this baseline simulation

with ≈500 ppm of CO_2, we have performed an equilibrium simulation with ≈1,165 ppm for sensitivity tests (see supporting information).

The simulated global annual mean surface air temperature for the late-Cretaceous climate state with ≈500 ppm of atmospheric CO_2 is 19.0°C, about 4°C higher than the pre-industrial temperature. Further discussion of this pre-impact state including figures for the temperature distribution as well as a description of the sensitivity simulation with a higher atmospheric CO_2 concentration can be found in the supporting information. The modeled global mean marine net primary productivity (NPP) for the pre-impact climate state is 48 GtC/year. In a late-Holocene configuration of the model, the simulated global mean marine NPP is about 27 GtC/year, at the lower end of the range of CMIP5 values (Fu et al., 2016), but well within the broad interval (50 ± 28 Gt C/year) of observational estimates (Malone et al., 2017).

2.3. Modeling the Climatic Effects of the Impact

We explore the effects of sulfate aerosols, carbon dioxide (CO_2) and dust produced by the Chicxulub impact on the climate and the marine biosphere. To model the radiative effect of the sulfate aerosols we use a time series of visible transmission for 2.1 years stratospheric residence time and for a load of 100 Gt S with 80% of the sulfur ligated as SO_2 and 20% as SO_3 (Brugger et al., 2017; Pierazzo et al., 2003). Note that more recent investigations with geophysical impact models suggest higher sulfur masses based on new limits for the impact angle and the target composition (Artemieva et al., 2017). However, as the radiative effect does not increase for sulfur loads larger than 30 Gt (Pierazzo et al., 2003), we do not consider the radiative effect of larger sulfur masses. In our standard simulations it is assumed that sulfate aerosols are transferred directly to the ocean after leaving the stratosphere (Pierazzo et al., 2003), with 100% of the sulfur passed to the ocean. To derive a time sequence for the sulfur flux to the ocean we use data for the stratospheric sulfate aerosol concentration decreasing over 6 years (Pierazzo et al., 2003) to calculate the monthly flux to the ocean. We also test the influence of additional sulfur deposition to the ocean on shorter timescales of 10 days after the impact as it was suggested that sulfate aerosols are scavenged by larger and faster settling silicate particles (Ohno et al., 2014; Tyrrell et al., 2015).

Additionally, we consider the atmospheric and oceanic effects of an increased atmospheric CO_2 concentration due to the impact. For our standard impact simulation we use an additional carbon mass of 115 Gt. This represents the carbon release primarily from the vapourization of carbonate rocks (Artemieva et al., 2017). CO_2 is equally distributed over 10 days after the impact assuming instantaneous formation. As for the sulfate aerosols, a globally uniform distribution is used. We also test the sensitivity to C masses between 0 and 4,115 Gt (Artemieva et al., 2017; Pierazzo et al., 1998, 2003; Tyrrell et al., 2015), considering additional C from wildfires (additional 1,500 Gt) and decomposed soil organic carbon (additional 2,500 Gt assuming to be instantaneously released, Tyrrell et al., 2015). We use $\delta^{13}C$ values of −3‰ for the C from the carbonate rocks (Kettrup et al., 2000) and −27‰ for C from organic material, assuming a plant mixture of C_3 and C_3+CAM plants (Gilman & Edwards, 2020; Osborne & Sack, 2012).

As it was shown that the radiative effects of impact dust were dominated by the effects of sulfate aerosols (Pierazzo et al., 2003; Pope, 2002) and possibly soot (Bardeen et al., 2017), we only consider the effects of the impact dust from the projectile on the ocean, in particular from the important nutrients iron and phosphorus. We explicitly model the atmospheric transport and deposition of impact dust from the projectile to derive the dust distribution in the ocean. To estimate the amount of iron and phosphor distributed in the ocean, we assume that the impactor was a carbonaceous chondrite of type CV, CO or CR (Kyte, 1998). These chondrites have typical iron and phosphorus fractions of 22.5% and 0.104%, respectively (Braukmüller et al., 2018). The modeling of the dust distribution and transport as well as the increase of the bioavailability after the impact is described in detail in the supporting information. For sensitivity tests, we also run the standard impact simulation (115 Gt C and 100 Gt S) and an impact simulation with additional 1,500 Gt C for the pre-impact state with 1,165 ppm of CO_2.

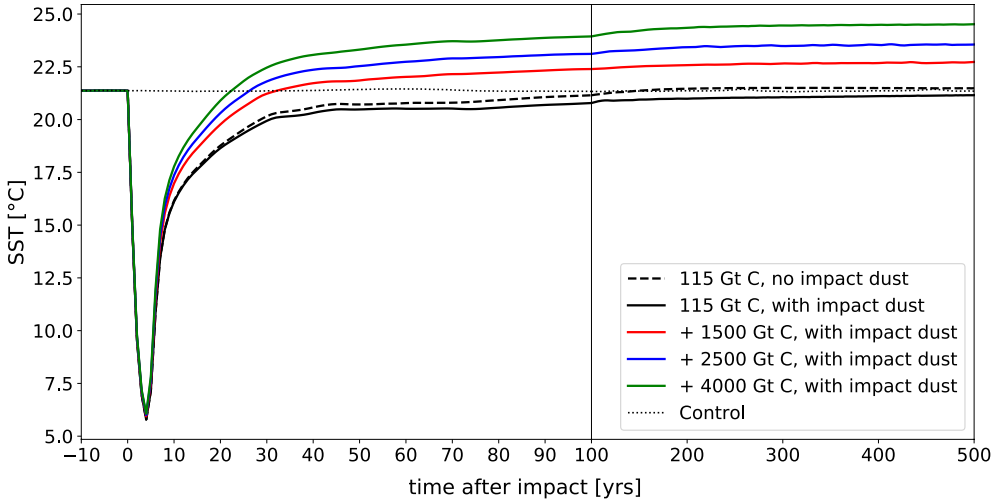

Figure 1. Sea surface temperature evolution for different amounts of carbon released due to the impact. Annual and global mean sea surface temperature before and after the impact for simulations with (solid lines) and without the effects of dust produced during the impact (dashed line) as well as for different amounts of organic carbon released from terrestrial reservoirs (colored lines).

3. Results

3.1. Temperature Changes in the Millennium After the Impact

The strong reduction in incoming solar radiation due to the stratospheric sulfate aerosols from the impact (Brugger et al., 2017; Pierazzo et al., 2003) has far-reaching implications for climate and life. This is most evident in the severe global cooling in the first decades after the impact. Global annual mean sea surface temperatures (SSTs) are reduced from 21.4°C by about ~15°C in the fourth year after the impact (Figure 1). Temperatures recover over the following centuries, approaching pre-impact values after 1,000 years. For a higher late-Cretaceous CO_2 concentration, the impact induces a cooling of very similar magnitude in the immediate aftermath of the impact. More detailed results and discussion for the impact simulations with higher CO_2 concentration can be found in the supporting information (Table S1, Figures S9–S11 and supporting information S5).

Tracing the decadal-scale cooling induced by the impact in geological records is challenging. However, high-resolution proxy data for the Brazos River region (Vellekoop et al., 2014) and for the New Jersey shelf region (Vellekoop et al., 2016) indicate cooling of 7°C (resolved on timescales of months to decades) and 3°C (resolved on timescales of decades to centuries), respectively, in good agreement with the cooling simulated in our model and averaged over appropriate timescales (see Table S1 in supporting information). Furthermore, the data for the Brazos region (Vellekoop et al., 2014, 2018) indicate a long-term increase of SST of 1−2°C in the early Paleogene starting in the centuries after the impact. In our simulations, the amplitude of SST changes at this location is very similar to the global value; therefore we can directly compare the global SST curves shown in Figure 1 with the proxy estimates. With carbon emissions from the impact only (and the response of the marine biosphere), our standard simulation shows no significant warming in the centuries after the impact. However, one would expect additional carbon emissions from the terrestrial biosphere (e.g., from dying vegetation, wildfires, or soil decomposition) which are not taken into account in this model experiment. Simulations with a series of larger carbon emissions (Figure 1) show that the best agreement with the Brazos River proxy data is achieved for additional 1,500 Gt C from terrestrial sources for the late-Cretaceous simulations with 500 ppm atmospheric CO_2 concentration. For a higher pre-impact CO_2 level, the long-term warming after the impact is smaller for the same amount of additional carbon (see Table S1, Figure S9 and supporting information S5), which is to be expected for a significantly higher baseline CO_2 concentration. Therefore, if the late-Cretaceous atmospheric CO_2 concentration was higher than 500 ppm, the proxy comparison for the pre-impact warming suggests the addition of even more carbon from terrestrial sources. A decrease of 1.2‰ in $\delta^{18}O$ of fine fraction carbonate for Caravaca, Spain, in the

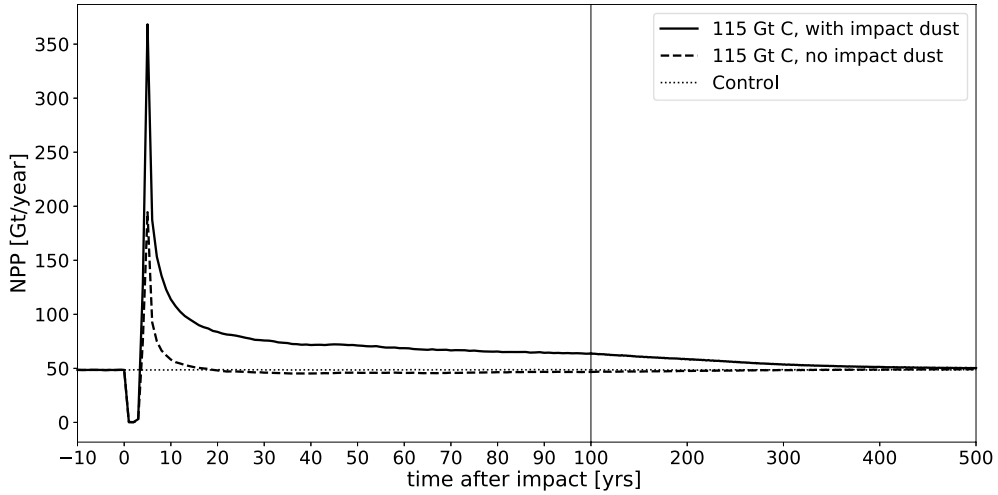

Figure 2. Effects of the impact on the marine biosphere. Annual and global mean ocean net primary productivity before and after the impact for simulations with (solid line) and without the effects of dust produced during the impact (dashed line).

centuries and first millennia after the impact (Kaiho et al., 1999) also supports a warming after the impact, but the suggested strong warming of ~5°C (Kaiho et al., 1999) is highly uncertain due to diagenesis, the superposition of different vital effects (e.g., Ziveri et al., 2003) linked to the complex composition of fine fraction carbonate, and the fact that $\delta^{18}O$ of sea water is not constrained.

3.2. A Brief Peak of Net Primary Productivity After the Impact

The Chicxulub impact had profound short-term repercussions for the marine biosphere. In our simulations, the global annual mean NPP in the ocean drops to almost zero in the three years following the impact before briefly peaking at a maximum value about a factor of seven higher than the pre-impact NPP (Figure 2). Although the NPP peak lasts only for a few years, higher productivity persists for decades to centuries, returning to pre-impact levels only after ~500 years.

The almost complete shutdown of marine NPP in the first years after the impact is caused by both the low light levels and the resulting temperature decrease. With the solar flux starting to recover already two years after the impact and reaching its pre-impact value after seven years (Brugger et al., 2017), global annual mean marine NPP exceeds pre-impact levels of 48 Gt/year in the fourth year after the impact and culminates in a sharp peak at a value of 368 Gt/year in year five. This increase in NPP is caused by two mechanisms: First, the severe surface cooling of the ocean following the impact induces strong ocean mixing and deep water formation, leading to a deep mixed layer, in particular in the mid-latitudes (see supporting information and Brugger et al. (2017) for figures and further discussion). This results in the transport of a large amount of nutrients from the deep ocean to the surface, thus increasing the productivity. Second, considerable amounts of iron and phosphorus are delivered to the ocean by the impact dust originating from the iron-rich projectile. These nutrients with increased bioavailability (see Section 2.3 and supporting information) are sufficient to sustain elevated levels of the NPP for several centuries. In contrast, the nutrients brought to the surface ocean by deep mixing are quickly consumed, as shown by a simulation without dust from the impact (see Figure 2).

The uptake of large amounts of carbon during the period of high ocean productivity results in lower atmospheric CO_2 concentrations and consequently decreases temperatures. Hence, earlier simulations without marine biogeochemistry show a very similar cooling, but a faster recovery where pre-impact temperatures are exceeded already after less than 100 years (Brugger et al., 2017).

Regionally, the increase in marine NPP starts in the tropics where light and ocean temperature exceed the critical thresholds necessary for photosynthesis earliest (Figure S1 in supporting information). As the cooling of the ocean's surface induces strong ocean mixing in particular in the mid-latitudes (Brugger

et al., 2017) bringing large amounts of nutrients to the surface ocean, the high primary productivity quickly expands to these regions. The nutrients from the impact dust are quickly spread in the ocean and hence do not cause significant local effects, but amplify the regional NPP patterns also observed in the simulation without impact dust. NPP stays below its pre-impact value for more than 10 years after the impact only in the very high Northern latitudes as a result of the very low ocean temperatures in this region. Note that productivity in coastal regions could have been even higher due to nutrient input from the terrestrial biosphere (Vellekoop et al., 2018) not taken into account in our model.

Blooms of dinoflagellates and cyanobacteria associated with regional maxima in the NPP could result in the production of toxins with detrimental effects for marine near-surface ecosystems. This mechanism described here for the first time could thus play a role in the context of the immediate effects of the impact on the marine biosphere. We note that the increased marine productivity might be dampened by self-limiting feedbacks of the algal bloom (Jackson & Lochmann, 1992; Shigesada & Okubo, 1981) which are not represented in our model. Another aspect not considered here is the formation of cloud condensation nuclei as a consequence of algal blooms. Planktonic algae produce dimethylsulfide (DMS) which form sulfate aerosols in the atmosphere acting as cloud condensation nuclei. Higher densities of cloud condensation nuclei influence cloud albedo and lifetime, and could therefore prolong the cooling after the impact (Charlson et al., 1987; Feulner et al., 2015).

Although there are no empirical data on the productivity immediately after the impact, it has been suggested that marine primary productivity could have been strongly limited only during the short period with direct environmental consequences of the impact, potentially only for a decade (D'Hondt, 2005), consistent with our results. A combined interpretation of proxy data, the fossil record and model results indicates that marine primary productivity recovered to normal or regionally high values (Hollis et al., 1995, 2003; Lowery et al., 2020; Sepúlveda et al., 2009, 2019; Vellekoop et al., 2017, 2018) much earlier than the biological pump, but that the remineralization depth of organic matter was shallower, leading to a decrease in the export productivity ("Living Ocean" hypothesis, D'Hondt et al., 1998). Estimates for the recovery time for the marine primary productivity are constrained by the age models of the proxy studies and vary between a century (Sepúlveda et al., 2009), and tens of thousands of years (Henehan et al., 2019; Sepúlveda et al., 2019). Hence, our results suggest a convincing scenario for the immediate effect of the impact on primary productivity which cannot be resolved by proxy data and fits the observation of regionally heterogenous recovery of productivity (Sepúlveda et al., 2019). Nevertheless, there might have been some additional, prolonged effects limiting primary productivity in the centuries to millennia after the boundary, both as consequences of the impact as well as other changes across the boundary (Arthur et al., 1987), which are not represented in our model.

3.3. Carbon Isotopes Suggest Significant Release of Terrestrial Carbon

The strong perturbations at the K-Pg boundary induce severe changes in the marine carbon cycle leaving traces in the ocean's dissolved inorganic carbon $\delta^{13}C$ values. This signal depends both on the amount of carbon emitted due to the impact and on its isotopic signature; it is therefore important to assign appropriate $\delta^{13}C$ values to modeled carbon fluxes from different sources (see Section 2.3). We find an immediate reduction of $\delta^{13}C$ in the surface ocean (Figure 3 for the region around Shatsky Rise in the Northern Pacific). The decrease is caused by the enhanced ocean mixing transporting inorganic C with lower $\delta^{13}C$ from the deeper ocean to the surface, combined with the reduced primary productivity in the first years after the impact. These processes dominate the simulation with only 115 Gt C: after a short decrease $\delta^{13}C$ starts to rise during the productivity maximum before approaching a new equilibrium slightly above the pre-impact value. In contrast, $\delta^{13}C$ values in the simulations with carbon released from the terrestrial biosphere are determined by these additional amounts of isotopically light carbon, decreasing the ocean's $\delta^{13}C$ significantly. Surface $\delta^{13}C$ starts to increase and approaches a new equilibrium value when the added carbon is exported to the deeper ocean. Hence, the reduction of $\delta^{13}C$ in the deep ocean is smaller and delayed compared to the surface ocean, resulting in a reduced $\delta^{13}C$ gradient from the surface to the deep ocean.

The immediate effect of the Chicxulub impact on $\delta^{13}C$ in the first millennium after the event are resolved in detail in our simulations, but not covered by proxy data due to a lack of temporal resolution. However, if we interpret the earliest surface proxy data after the impact as a smeared signal for the time since the K-Pg

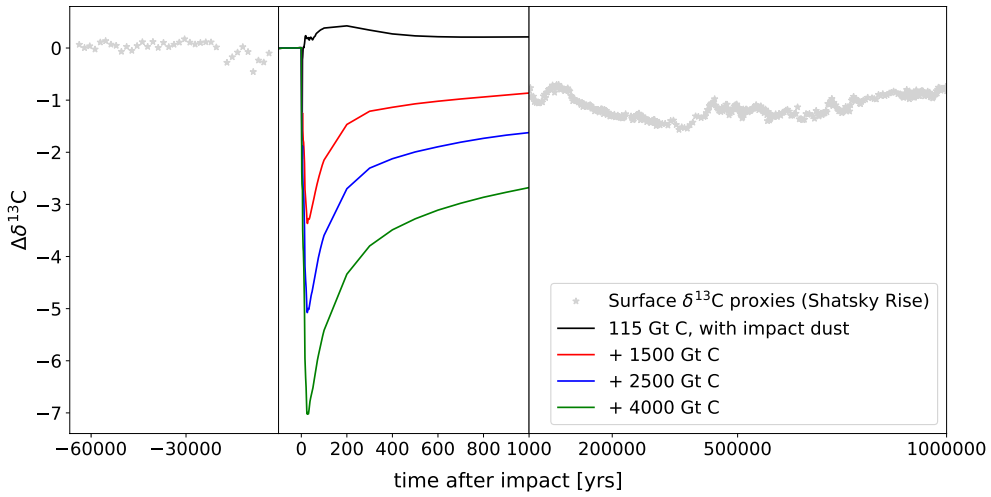

Figure 3. Changes of surface carbon isotope ratios of dissolved inorganic carbon at Shatsky Rise, Pacific. Colored lines show modeled changes in $\delta^{13}C$ for the 1,000 years after the impact relative to the 100-year pre-impact mean for simulations with different amounts of carbon. The model results are embedded in changes in surface $\delta^{13}C$ from proxy data from bulk carbonate (Table S11 in Hull et al., 2020), assuming an absolute age for the K-Pg boundary of 66.022 Ma (Table S3 in Hull et al., 2020) relative to the mean of the pre-impact proxy values.

boundary, again our simulation with an additional amount of 1,500 Gt C from the terrestrial biosphere shows the best agreement with the proxy data (see Figure 3), confirming the release of significant quantities of carbon from the terrestrial biosphere already suggested by the temperature evolution. This finding also holds for a significantly higher atmospheric CO_2 concentration before the impact (see Figure S10 in the supporting information). We note that a comparison of modeled $\delta^{13}C$ data for the deep ocean with benthic proxy data is challenging because of the higher variability and lower temporal resolution of the benthic $\delta^{13}C$ data for this period (Henehan et al., 2019; Hull et al., 2020).

3.4. Moderate Ocean Acidification Followed by a Fast Recovery

The paleontologic record of the end-Cretaceous shows a significantly higher extinction rate of marine calcifying organisms (Tyrrell et al., 2015). This could be a consequence of ocean acidification caused by the fast release of CO_2 and H_2SO_4 during the impact. However, the occurrence of an acidified ocean is still debated, as the observed extinction patterns differ strongly among different calcifying species, making it difficult to get a clear understanding of the extent of acidification and its effects on the biosphere (D'Hondt, 2005; Dishon et al., 2020; Kiessling & Baron-Szabo, 2004; Kiessling & Simpson, 2011; Tyrrell et al., 2015).

To explore the influence of impact-related carbon and sulfur emissions, we model their effects on the ocean's carbonate saturation state and pH. Consistent with our findings from the changes in temperature and $\delta^{13}C$, we assume an additional carbon amount of 1,500 Gt C; for sulfur, we use the most recent estimate of 325 Gt S (Artemieva et al., 2017). Model experiments with higher C and S masses are discussed in the SI (Section 3 and Figures S2, S4 and S5).

We find an immediate reduction of surface global mean pH, with a maximum surface pH decrease of 0.36 units four years after the impact (see Figure S2 in supporting information). The subsequent emerging peak in ocean productivity and the accompanying high carbon uptake leads to a short increase in pH before it decreases again. These fast changes immediately after the impact are followed by a transient recovery over the next 500 years, equilibrating at 0.23 pH units below the pre-impact value. Data from the Geulhemmerberg succession show a pH reduction of ~0.25 for the millennium following the impact, but possibly even for a shorter time scale of ~100 years (Henehan et al., 2019). This is in excellent agreement with our modeled pH reduction of 0.28 pH units in this region averaged over the century after the impact.

To assess the influence on calcifiers, Figure 4 shows the surface ocean aragonite saturation state Ω_a. The critical value for the saturation state Ω varies for different calcifying species (Ries et al., 2009) and depends

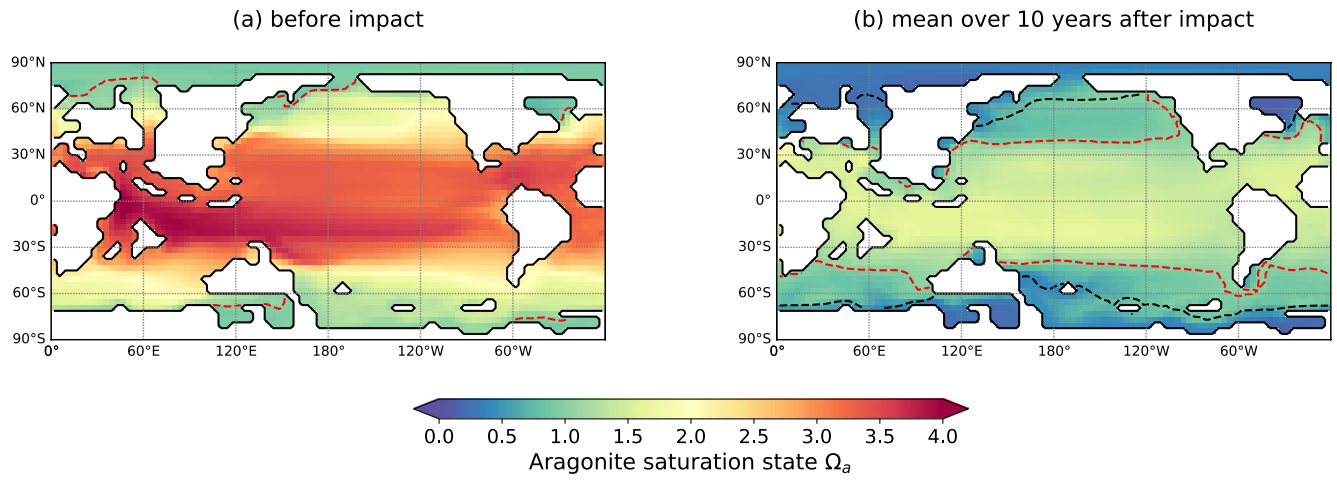

Figure 4. Effects of carbon and sulfur emissions from the impact on ocean acidification. Surface ocean aragonite saturation state before the impact (a) and for the average over the 10 years after the impact. The $\Omega_a = 1$ line is shown in red. The dashed black line in (b) shows $\Omega_a = 1$ for the 1,000 years after the impact.

on marine carbonate chemistry (Bach et al., 2015). Here we assume that calcifying organisms begin to dissolve for $\Omega < 1$. Globally, Ω_a is strongly reduced in the 10 years after the impact, and it falls below the critical value of 1 at latitudes higher than ~40°. Although Ω_a quickly starts to recover and the line defining $\Omega_a = 1$ retrenches to higher latitudes, Ω_a globally stays below the pre-impact values in the 1,000 years after the impact. The calcite saturation state Ω_c, which is generally higher than Ω_a due to the lower solubility of calcite in ocean water, shows similar patterns (see Figure S3 in supporting information). Ω_c falls below the critical value of 1 for latitudes greater than ~60° averaged for the 10 years after the impact before $\Omega_c = 1$ retrenches to higher latitudes.

In summary, we find rapid surface ocean acidification which, however, recovers quickly. The potential habitat for calcifiers after the impact is restricted to lower latitudes. For corals and rudists favoring warm waters, however, it is hard to distinguish whether the strong temperature decrease or the aragonitic undersaturation was more critical in limiting their habitat. As the surface ocean is undersaturated in calcite only at high latitudes, the global extinction of planktic foraminifera (D'Hondt, 2005) is difficult to explain primarily with ocean acidification. Our results thus indicate that surface ocean acidification after the Chicxulub impact caused regionally the extinction of some groups of calcifiers. However, the extinction of a large fraction of globally distributed calcifiers, as observed in the fossil record, cannot be caused by undersaturation alone, because it was not widespread enough.

4. Discussion

Our modeling results for the immediate consequences of the Chicxulub impact on the climate and the marine biosphere indicate rapid cooling, a sharp and short-lived increase of marine primary productivity following a brief productivity collapse, and moderate ocean acidification. The longer-term warming trend observed in proxy data and the comparison of surface $\delta^{13}C$ data with our model results suggest an additional carbon release of ~1,500 Gt from the terrestrial biosphere. If the carbon is the result of wildfires caused by the infrared radiation of the reentering ejecta (Robertson et al., 2013), the produced soot would have further reduced the incoming surface short wave radiation with significant effects on photosynthesis (Bardeen et al., 2017; Tabor et al., 2020). In addition, nutrients brought into the ocean by the wildfire ash could have intensified and prolonged the increase in marine primary productivity and the algal bloom (Abram et al., 2003). Proxy data indicate an additional nutrient flux resulting from land-derived material during the terrestrial mass extinction, leading in particular to increased productivity in the neritic zone during the centuries to millennia following the K-Pg boundary (Vellekoop et al., 2018). Future modeling studies will have to explore the full range of interactions between climate and the terrestrial and marine biosphere.

Recent studies on the interaction of Deccan volcanism and the Chicxulub impact support the notion that the impact was the major driver of the end-Cretaceous mass extinction (Hull et al., 2020; Sprain et al., 2019). From these findings and our results we conclude that the combination of several abrupt and vigorous changes caused by the Chicxulub impact triggered the end-Cretaceous mass extinction. In addition, life-history traits (D'Hondt, 2005), geographic distribution (Dishon et al., 2020), the respective ecosystem (D'Hondt, 2005) and chance survival (D'Hondt, 2005) could have determined the selectivity during the extinction. The interaction of these ecological and evolutionary factors with the modeled direct consequences of the impact would have to be further investigated, for example with ecological niche models.

Data Availability Statement

All model input and output files as well as the preprocessing and postprocessing scripts used to generate model input and the figures in the study are available online (https://doi.org/10.5880/PIK.2020.008). The source code for the model used in this study is archived at the Potsdam Institute for Climate Impact Research and is made available upon request.

Acknowledgments
The authors would like to thank Eva Bauer who laid the foundation for the implementation of dust production and transport in our model, Rosie Sheward and David Evans for their help with the interpretation of proxy data, and Johan Vellekoop and one anonymous reviewer for very helpful comments. The authors gratefully acknowledge the European Regional Development Fund (ERDF), the German Federal Ministry of Education and Research and the Land Brandenburg for supporting this project by providing resources on the high performance computer system at the Potsdam Institute for Climate Impact Research. The work was partly funded by the German Federal Ministry of Education and Research BMBF within the Collaborative Project "Bridging in Biodiversity Science – BIBS" (funding number 01LC1501A-H) and the VeWA consortium (Past Warm Periods as Natural Analogues of our high-CO_2 Climate Future) by the LOEWE programme of the Hessen Ministry of Higher Education, Research and the Arts, Germany. J.B. acknowledges support by a PhD Completion Grant from the Potsdam Graduate School.

References

Abram, N. J., Gagan, M. K., McCulloch, M. T., Chappell, J., & Hantoro, W. S. (2003). Coral reef death during the 1997 Indian Ocean dipole linked to Indonesian wildfires. *Science*, *301*(5635), 952–955. https://doi.org/10.1126/science.1083841

Alvarez, L. W., Alvarez, W., Asaro, F., & Michel, H. V. (1980). Extraterrestrial cause for the cretaceous-tertiary extinction. *Science*, *208*(4448), 1095–1108. https://doi.org/10.1126/science.208.4448.1095

Artemieva, N., Morgan, J., & Party, E. S. (2017). Quantifying the release of climate-active gases by large meteorite impacts with a case study of Chicxulub. *Geophysical Research Letters*, *44*(20), 10180–10188. https://doi.org/10.1002/2017GL074879

Arthur, M., Zachos, J., & Jones, D. (1987). Primary productivity and the Cretaceous/Tertiary boundary event in the oceans. *Cretaceous Research*, *8*(1), 43–54. https://doi.org/10.1016/0195-6671(87)90011-5

Bach, L. T., Riebesell, U., Gutowska, M. A., Federwisch, L., & Schulz, K. G. (2015). A unifying concept of coccolithophore sensitivity to changing carbonate chemistry embedded in an ecological framework. *Progress in Oceanography*, *135*, 125–138. https://doi.org/10.1016/j.pocean.2015.04.012

Bahcall, J. N., Pinsonneault, M. H., & Basu, S. (2001). Solar models: Current epoch and time dependences, neutrinos, and helioseismological properties. *The Astrophysical Journal*, *555*(2), 990–1012. https://doi.org/10.1086/321493

Bambach, R. K. (2006). Phanerozoic biodiversity mass extinctions. *Annual Review of Earth and Planetary Sciences*, *34*, 127–155. https://doi.org/10.1146/annurev.earth.33.092203.122654

Bardeen, C. G., Garcia, R. R., Toon, O. B., & Conley, A. J. (2017). On transient climate change at the Cretaceous-Paleogene boundary due to atmospheric soot injections. *Proceedings of the National Academy of Sciences of the United States of America*, *114*, E7415–E7424. https://doi.org/10.1073/pnas.1708980114

Bauer, E., & Ganopolski, A. (2010). Aeolian dust modeling over the past four glacial cycles with CLIMBER-2. *Global and Planetary Change*, *74*, 49–60. https://doi.org/10.1016/j.gloplacha.2010.07.009

Braukmüller, N., Wombacher, F., Hezel, D. C., Escoube, R., & Münker, C. (2018). The chemical composition of carbonaceous chondrites: Implications for volatile element depletion, complementarity and alteration. *Geochimica et Cosmochimica Acta*, *239*, 17–48. https://doi.org/10.1016/j.gca.2018.07.023

Brugger, J., Feulner, G., Hofmann, M., & Petri, S. (2021). Model data for simulations of ocean biogeochemistry after the Chicxulub impact. *GFZ Data Services*, https://doi.org/10.5880/PIK.2020.008

Brugger, J., Feulner, G., & Petri, S. (2017). Baby, it's cold outside: Climate model simulations of the effects of the asteroid impact at the end of the Cretaceous. *Geophysical Research Letters*, *44*(1), 419–427. https://doi.org/10.1002/2016GL072241

Charlson, R. J., Warren, S. G., Lovelock, J. E., & Andreae, M. O. (1987). Oceanic phytoplankton, atmospheric sulphur, cloud albedo and climate. *Nature*, *326*, 655–661. https://doi.org/10.1038/326655a0

Collins, G. S., Patel, N., Davison, T. M., Rae, A. S. P., Morgan, J. V., Gulick, S. P. S., et al. (2020). A steeply-inclined trajectory for the Chicxulub impact. *Nature Communications*, *11*. https://doi.org/10.1038/s41467-020-15269-x

D'Hondt, S. (2005). Consequences of the Cretaceous/Paleogene mass extinction for marine ecosystems. *Annual Review of Ecology, Evolution and Systematics*, *36*, 295–317. https://doi.org/10.1146/annurev.ecolsys.35.021103.105715

D'Hondt, S., Donaghay, P., Zachos, J. C., Luttenberg, D., & Lindinger, M. (1998). Organic carbon fluxes and ecological recovery from the Cretaceous-Tertiary mass extinction. *Science*, *282*, 276–279. https://doi.org/10.1126/science.282.5387.276

Dishon, G., Grossowicz, M., Krom, M., Guy, G., Gruber, D. F., & Tchernov, D. (2020). Evolutionary traits that enable Scleractinian corals to survive mass extinction events. *Scientific Reports*, *10*(10), 3903. https://doi.org/10.1038/s41598-020-60605-2

Ernst, R. E., & Youbi, N. (2017). How large Igneous provinces affect global climate, sometimes cause mass extinctions, and represent natural markers in the geological record. *Palaeogeography, Palaeoclimatology, Palaeoecology*, *478*, 30–52. https://doi.org/10.1016/j.palaeo.2017.03.014

Feulner, G., Hallmann, C., & Kienert, H. (2015). Snowball cooling after algal rise. *Nature Geoscience*, *8*, 659–662. https://doi.org/10.1038/ngeo2523

Feulner, G., & Kienert, H. (2014). Climate simulations of Neoproterozoic snowball Earth events: Similar critical carbon dioxide levels for the Sturtian and Marinoan glaciations. *Earth and Planetary Science Letters*, *404*, 200–205. https://doi.org/10.1016/j.epsl.2014.08.001

Fichefet, T., & Maqueda, M. A. M. (1997). Sensitivity of a global sea ice model to the treatment of ice thermodynamics and dynamics. *Journal of Geophysical Research*, *102*(C6), 12609–12646. https://doi.org/10.1029/97JC00480

Foster, G. L., Royer, D. L., & Lunt, D. J. (2017). Future climate forcing potentially without precedent in the last 420 million years. *Nature Communications*, *8*, 14845. https://doi.org/10.1038/ncomms14845

Fu, W., Randerson, J. T., & Moore, J. K. (2016). Climate change impact on net primary production (NPP) and export production (EP) regulated by increasing stratification and phytoplankton community structure in the CMIP5 models. *Biogeosciences*, *13*, 5151–5170. https://doi.org/10.5194/bg-13-5151-2016

Garcia, H. E., Weathers, K., Paver, C. R., Smolyar, I., Boyer, T. P., Locarnini, R. A., & Reagan, J. R. d. (2018). World ocean Atlas 2018, Volume 4: Dissolved inorganic nutrients (phosphate, nitrate and nitrate+nitrite, silicate). In Mishonov Technical, A. (Ed.), *NOAA Atlas NESDIS* (Vol. 84), NOAA.

Gilman, I. S., & Edwards, E. J. (2020). Crassulacean acid metabolism. *Current Biology*, *30*(2), R57–R62. https://doi.org/10.1016/j.cub.2019.11.073

Gulick, S. P. S., Bralower, T. J., Ormö, J., Hall, B., Grice, K., Schaefer, B., et al. (2019). The first day of the Cenozoic. *Proceedings of the National Academy of Sciences of the United States of America*, *116*(39), 19342–19351. https://doi.org/10.1073/pnas.1909479116

Henehan, M. J., Ridgwell, A., Thomas, E., Zhang, S., Alegret, L., Schmidt, D. N., et al. (2019). Rapid ocean acidification and protracted Earth system recovery followed the end-Cretaceous Chicxulub impact. *Proceedings of the National Academy of Sciences of the United States of America*, *116*(45), 22500–22504. https://doi.org/10.1073/pnas.1905989116

Hofmann, M., Broecker, W. S., & Lynch-Stieglitz, J. (1999). Influence of a [CO_2(aq)] dependent biological C-isotope fractionation on glacial 13C/12C ratios in the ocean. *Global Biogeochemical Cycles*, *13*, 873–883. https://doi.org/10.1029/1999GB900063

Hofmann, M., Mathesius, S., Kriegler, E., van Vuuren, D., & Schellnhuber, H. J. (2019). Strong time dependence of ocean acidification mitigation by atmospheric carbon dioxide removal. *Nature Communications*, *10*, 5592. https://doi.org/10.1038/s41467-019-13586-4

Hofmann, M., & Morales Maqueda, M. A. (2006). Performance of a second-order moments advection scheme in an Ocean General Circulation Model. *Journal of Geophysical Research*, *111*, C05006. https://doi.org/10.1029/2005JC003279

Hollis, C. J., Rodgers, K. A., & Parker, R. J. (1995). Siliceous plankton bloom in the earliest Tertiary of Marlborough, New Zealand. *Geology*, *23*(9), 835–838. https://doi.org/10.1130/0091-7613(1995)023<0835:SPBITE>2.3.CO;2

Hollis, C. J., Rodgers, K. A., Strong, C. P., Field, B. D., & Rogers, K. M. (2003). Paleoenvironmental changes across the Cretaceous/Tertiary boundary in the northern Clarence valley, southeastern Marlborough, New Zealand. *New Zealand Journal of Geology and Geophysics*, *46*(2), 209–234. https://doi.org/10.1080/00288306.2003.9515005

Hong, S. K., & Lee, Y. I. (2012). Evaluation of atmospheric carbon dioxide concentrations during the Cretaceous. *Earth and Planetary Science Letters*, *327*, 23–28. https://doi.org/10.1016/j.epsl.2012.01.014

Hull, P. M., Bornemann, A., Penman, D. E., Henehan, M. J., Norris, R. D., Wilson, P. A., et al. (2020). On impact and volcanism across the Cretaceous-Paleogene boundary. *Science*, *367*(6475), 266–272. https://doi.org/10.1126/science.aay5055

Jackson, G. A., & Lochmann, S. E. (1992). Effect of coagulation on nutrient and light limitation of an algal bloom. *Limnology & Oceanography*, *37*(1), 77–89. https://doi.org/10.4319/lo.1992.37.1.0077

Kaiho, K., Kajiwara, Y., Tazaki, K., Ueshima, M., Takeda, N., Kawahata, H., et al. (1999). Oceanic primary productivity and dissolved oxygen levels at the Cretaceous/Tertiary Boundary: Their decrease, subsequent warming, and recovery. *Paleoceanography*, *14*(4), 511–524. https://doi.org/10.1029/1999PA900022

Kettrup, B., Deutsch, A., Ostermann, M., & Agrinier, P. (2000). Chicxulub impactites: Geochemical clues to the precursor rocks. *Paleoceanography*, *35*, 1229–1238. https://doi.org/10.1111/j.1945-5100.2000.tb01511.x

Key, R. M., Kozyr, A., Sabine, C. L., Lee, K., Wanninkhof, R., Bullister, J. L., et al. (2004). A global ocean carbon climatology: Results from Global Data Analysis Project (GLODAP). *Global Biogeochemical Cycles*, *18*(4), GB4031. https://doi.org/10.1029/2004GB002247

Kiessling, W., & Baron-Szabo, R. (2004). Extinction and recovery patterns of scleractinian corals at the Cretaceous-Tertiary boundary. *Palaeogeography, Palaeoclimatology, Palaeoecology*, *214*(3), 195–223. https://doi.org/10.1016/j.palaeo.2004.05.025

Kiessling, W., & Simpson, C. (2011). On the potential for ocean acidification to be a general cause of ancient reef crises. *Global Change Biology*, *17*(1), 56–67. https://doi.org/10.1111/j.1365-2486.2010.02204.x

Kopp, G., & Lean, J. L. (2011). A new, lower value of total solar irradiance: Evidence and climate significance. *Geophysical Research Letters*, *38*(1), L01706. https://doi.org/10.1029/2010GL045777

Kring, D. A. (2007). The Chicxulub impact event and its environmental consequences at the Cretaceous-Tertiary boundary. *Palaeogeography, Palaeoclimatology, Palaeoecology*, *255*(1–2), 4–21. https://doi.org/10.1016/j.palaeo.2007.02.037

Kyte, F. T. (1998). A meteorite from the Cretaceous/Tertiary boundary. *Nature*, *396*, 237–239. https://doi.org/10.1038/24322

Lowery, C. M., Bown, P. R., Fraass, A. J., & Hull, P. M. (2020). Ecological response of plankton to environmental change: Thresholds for extinction. *Annual Review of Earth and Planetary Sciences*, *48*(1), 403–429. https://doi.org/10.1146/annurev-earth-081619-052818

Maier-Reimer, E. (1993). Geochemical cycles in an ocean general circulation model. Preindustrial tracer distributions. *Global Biogeochemical Cycles*, *7*, 645–677. https://doi.org/10.1029/93GB01355

Malone, T., Azzaro, M., Bode, A., Brown, E., Calumpong, H., Duce, R., & Wang, J. (2017). Primary production, cycling of nutrients, surface layer and plankton. In United Nations (Ed.), *The first global integrated marine Assessment, World ocean Assessment I* (pp. 119–148). Cambridge University Press. https://doi.org/10.1017/9781108186148

Montoya, M., Griesel, A., Levermann, A., Mignot, J., Hofmann, M., Ganopolski, A., & Rahmstorf, S. (2005). The Earth system model of intermediate complexity CLIMBER-3α. Part I: Description and performance for present-day conditions. *Climate Dynamics*, *25*(2–3), 237–263. https://doi.org/10.1007/s00382-005-0044-1

Nordt, L., Atchley, S., & Dworkin, S. (2002). Paleosol barometer indicates extreme fluctuations in atmospheric CO_2 across the Cretaceous-Tertiary boundary. *Geology*, *30*(8), 703–706. https://doi.org/10.1130/0091-7613(2002)030<0703:PBIEFI>2.0.CO;2

Nordt, L., Atchley, S., & Dworkin, S. (2003). Terrestrial evidence for two greenhouse events in the latest Cretaceous. *GSA Today*, *13*, 4–9. https://doi.org/10.1130/1052-5173(2003)013<4:teftge>2.0.co;2

Ohno, S., Kadono, T., Kurosawa, K., Hamura, T., Sakaiya, T., Shigemori, K., et al. (2014). Production of sulphate-rich vapor during the Chicxulub impact and implications for ocean acidification. *Nature Geoscience*, *7*, 279–282. https://doi.org/10.1038/ngeo2095

Osborne, C. P., & Sack, L. (2012). Evolution of C_4 plants: A new hypothesis for an interaction of CO_2 and water relations mediated by plant hydraulics. *Philosophical Transactions of the Royal Society B*, *367*(1588), 583–600. https://doi.org/10.1098/rstb.2011.0261

Pacanowski, R. C., & Griffies, S. M. (1999). *The MOM-3 manual* (Tech. Rep. No. 4). Princeton, NJ: GFDL Ocean Group, NOAA/Geophysical Fluid Dynamics Laboratory.

Petoukhov, V., Ganopolski, A., Brovkin, V., Claussen, M., Eliseev, A., Kubatzki, C., & Rahmstorf, S. (2000). CLIMBER-2: A climate system model of intermediate complexity. Part I: Model description and performance for present climate. *Climate Dynamics*, *16*(1), 1–17. https://doi.org/10.1007/PL00007919

Pierazzo, E., Hahmann, A. N., & Sloan, C. (2003). Chicxulub and climate: Radiative perturbations of impact-produced S-bearing gases. *Astrobiology*, *3*(1), 99–118. https://doi.org/10.1089/153110703321632453

Pierazzo, E., Kring, D. A., & Melosh, H. J. (1998). Hydrocode simulation of the Chicxulub impact event and the production of climatically active gases. *Journal of Geophysical Research*, *103*(E12), 28607–28625. https://doi.org/10.1029/98JE02496

Pope, K. O. (2002). Impact dust not the cause of the Cretaceous-Tertiary mass extinction. *Geology*, *30*(2), 99–102. https://doi.org/10.1130/0091-7613(2002)030<0099:idntco>2.0.co;2

Renne, P. R., Deino, A. L., Hilgen, F. J., Kuiper, K. F., Mark, D. F., Mitchell, W. S., et al. (2013). Time Scales of critical events Around the Cretaceous-Paleogene boundary. *Science*, *339*, 684–687. https://doi.org/10.1126/science.1230492

Ries, J. B., Cohen, A. L., & McCorkle, D. C. (2009). Marine calcifiers exhibit mixed responses to CO_2-induced ocean acidification. *Geology*, *12*(12), 1131–1134. https://doi.org/10.1130/G30210A.1

Robertson, D. S., Lewis, W. M., Sheehan, P. M., & Toon, O. B. (2013). K-Pg extinction: Reevaluation of the heat-fire hypothesis. *Journal of Geophysical Research: Biogeosciences*, *118*(1), 329–336. https://doi.org/10.1002/jgrg.20018

Royer, D. L. (2006). CO_2-forced climate thresholds during the Phanerozoic. *Geochimica et Cosmochimica Acta*, *70*(23), 5665–5675. https://doi.org/10.1016/j.gca.2005.11.031

Royer, D. L., Pagani, M., & Beerling, D. J. (2012). Geobiological constraints on Earth system sensitivity to CO_2 during the Cretaceous and Cenozoic. *Geobiology*, *10*(4), 298–310. https://doi.org/10.1111/j.1472-4669.2012.00320.x

Schmieder, M., & Kring, D. A. (2020). Earth's impact events through geologic time: A list of recommended ages for terrestrial impact structures and deposits. *Astrobiology*, *20*(1), 91–141. https://doi.org/10.1089/ast.2019.2085

Schoene, B., Eddy, M. P., Samperton, K. M., Keller, C. B., Keller, G., Adatte, T., & Khadri, S. F. R. (2019). U-Pb constraints on pulsed eruption of the Deccan Traps across the end-Cretaceous mass extinction. *Science*, *363*(6429), 862–866. https://doi.org/10.1126/science.aau2422

Schulte, P., Alegret, L., Arenillas, I., Arz, J. A., Barton, P. J., Bown, P. R., et al. (2010). The Chicxulub asteroid impact and mass extinction at the Cretaceous-Paleogene boundary. *Science*, *327*(5970), 1214–1218. https://doi.org/10.1126/science.1177265

Sepúlveda, J., Alegret, L., Thomas, E., Haddad, E., Cao, C., & Summons, R. E. (2019). Stable isotope constraints on marine productivity across the Cretaceous-Paleogene mass extinction. *Paleoceanography and Paleoclimatology*, *34*(7), 1195–1217. https://doi.org/10.1029/2018PA003442

Sepúlveda, J., Wendler, J. E., Summons, R. E., & Hinrichs, K.-U. (2009). Rapid resurgence of marine productivity after the Cretaceous-Paleogene mass extinction. *Science*, *326*(5949), 129–132. https://doi.org/10.1126/science.1176233

Sewall, J. O., van de Wal, R. S. W., van der Zwan, K., van Oosterhout, C., Dijkstra, H. A., & Scotese, C. R. (2007). Climate model boundary conditions for four Cretaceous time slices. *Climate of the Past*, *3*(4), 647–657. https://doi.org/10.5194/cp-3-647-2007

Shigesada, N., & Okubo, A. (1981). Analysis of the self-shading effect on algal vertical distribution in natural waters. *Journal of Mathematical Biology*, *12*(3), 311–326. https://doi.org/10.1007/BF00276919

Six, K., & Maier-Reimer, E. (1996). Effects of plankton dynamics on seasonal carbon fluxes in an ocean general circulation model. *Global Biogeochemical Cycles*, *10*, 559–583. https://doi.org/10.1029/96GB02561

Sprain, C. J., Renne, P. R., Vanderkluysen, L., Pande, K., Self, S., & Mittal, T. (2019). The eruptive tempo of Deccan volcanism in relation to the Cretaceous-Paleogene boundary. *Science*, *363*(6429), 866–870. https://doi.org/10.1126/science.aav1446

Tabor, C. R., Bardeen, C. G., Otto-Bliesner, B. L., Garcia, R. R., & Toon, O. B. (2020). Causes and climatic consequences of the impact winter at the Cretaceous-Paleogene boundary. *Geophysical Research Letters*, *47*(3), e60121. https://doi.org/10.1029/2019GL085572

Tyrrell, T., Merico, A., & Mckay, D. I. A. (2015). Severity of ocean acidification following the end Cretaceous asteroid impact. *Proceedings of the National Academy of Sciences of the United States of America*, *112*(21), 6556–6561. https://doi.org/10.1073/pnas.1418604112

Vellekoop, J., Esmeray-Senlet, S., Miller, K. G., Browning, J. V., Sluijs, A., van de Schootbrugge, B., et al. (2016). Evidence for Cretaceous–Paleogene boundary bolide "impact winter" conditions from New Jersey, USA. *Geology*, *44*(8), 619–622. https://doi.org/10.1130/G37961.1

Vellekoop, J., Sluijs, A., Smit, J., Schouten, S., Weijers, J. W. H., Sinninghe Damsté, J. S., & Brinkhuis, H. (2014). Rapid short-term cooling following the Chicxulub impact at the Cretaceous–Paleogene boundary. *Proceedings of the National Academy of Sciences of the United States of America*, *111*(21), 7537–7541. https://doi.org/10.1073/pnas.1319253111

Vellekoop, J., Woelders, L., Açikalin, S., Smit, J., van de Schootbrugge, B., Yilmaz, I. O., et al. (2017). Ecological response to collapse of the biological pump following the mass extinction at the Cretaceous–Paleogene boundary. *Biogeosciences*, *14*(4), 885–900. https://doi.org/10.5194/bg-14-885-2017

Vellekoop, J., Woelders, L., van Helmond, N. A., Galeotti, S., Smit, J., Slomp, C. P., et al. (2018). Shelf hypoxia in response to global warming after the Cretaceous-Paleogene boundary impact. *Geology*, *46*(8), 683–686. https://doi.org/10.1130/G45000.1

Zachos, J. C., Arthur, M. A., & Dean, W. E. (1989). Geochemical evidence for suppression of pelagic marine productivity at the Cretaceous/Tertiary boundary. *Nature*, *337*(6202), 61–64. https://doi.org/10.1038/337061a0

Ziveri, P., Stoll, H., Probert, I., Klaas, C., Geisen, M., Ganssen, G., & Young, J. (2003). Stable isotope 'vital effects' in coccolith calcite. *Earth and Planetary Science Letters*, *210*(1), 137–149. https://doi.org/10.1016/S0012-821X(03)00101-8